Analytical Electron Microscopy Studies of Lithium Aluminum Hydrides with Ti- and V-Based Additives

Carmen M. Andrei,[†] John C. Walmsley,[‡] Hendrik W. Brinks,[§] Randi Holmestad,*[,†] Didier Blanchard,[§] Bjørn C. Hauback,[§] and Gianluigi A. Botton[||]

Department of Physics, Norwegian University of Science and Technology, NTNU NO-7491 Trondheim, Norway, SINTEF Materials and Chemistry, NO-7465 Trondheim, Norway, Institute for Energy Technology, P. O. Box 40, NO-2027 Kjeller, Norway, and Department of Materials Science and Engineering, McMaster University, Hamilton, ON, L8S 4M1, Canada

Received: October 28, 2004; In Final Form: December 15, 2004

The microstructure of $LiAlD_4$ with $TiCl_3 \cdot 1/3(AlCl_3)$ and VCl_3 additives has been studied during different steps of the decomposition process using electron energy loss spectroscopy and energy-dispersive X-ray spectroscopy in a scanning transmission electron microscope. Energy filtered transmission electron microscopy was used to show elemental distributions in the samples. The spatial distribution of the additives and the main elements within the alanate particles was examined with a resolution of a few nanometers. The analysis of the electron energy loss spectra reveals the chemical state of Al, O, and the additives. Ti and V do not appear to mix chemically with Al to a significant degree. V was found in high concentration in just a few particles, while Ti is more uniformly distributed. All the samples showed evidence of oxidation despite procedures being adopted to avoid exposing the material to air. The additives are oxidized in all the samples, and Al_2O_3 forms a thin layer at the surface of the particles. This paper gives a comparison between samples at different stages of the decomposition process using different additives.

Introduction

Concerns over global warming and air pollution have stimulated the introduction of the "hydrogen economy" and the potential extensive use of hydrogen as an energy carrier, providing several environmental benefits. The major challenge today is to find a hydrogen storage system that can meet the constraints of volume, weight, safety, efficiency, and cost. One of the promising solutions is metal hydrides, but the gravimetric hydrogen capacity at around ambient temperature and atmospheric pressure is limited to less than 3 wt % for interstitial type metal hydrides, which is below the goal of the International Energy Agency (IEA) of minimum 5 wt %.

The use of complex hydrides containing aluminum (alanates) has several advantages over other metal hydride systems. Alanates are interesting because of their low molecular weight and the large amount of hydrogen per unit weight of storage material. Until recently, these potential benefits of alanates were overshadowed by the fact that they cannot be used to reversibly store hydrogen at moderate pressure and temperature. In 1997 Bogdanovic and Schwickardi showed that, by adding solution-based Ti catalysts, $NaAlH_4$ could be reversibly hydrided and dehydrided under moderate conditions.[1] Since then, complex hydrides have opened a new field of hydrogen storage materials and $NaAlH_4$ has been studied in particular detail. Later, it was reported that mechanical introduction of additive to $NaAlH_4$ also improved the hydrogenation/dehydrogenation process.[2,3] Furthermore, Zaluska and co-workers reported that preparation of sodium alanates by ball milling accelerates the reaction kinetics.[4] The role of the transition metal in the reaction kinetics as a catalyst or a dopant is still not yet understood, and we therefore simply describe it as an additive.

Lithium alanate, $LiAlH_4$, was first synthesized in 1947,[5] and since then several groups[6−13] have studied this system. However, there are still some open questions regarding the conditions for its reversibility. The hydrogen storage capacity of $LiAlH_4$ is very high, 10.6 wt % in total. Decomposition takes place in three steps upon heating[13−16] with 5.3, 2.6, and 2.6 wt % release of hydrogen, respectively:

$$3LiAlH_4 = Li_3AlH_6 + 2Al + 3H_2 \quad \text{(R1)}$$

$$Li_3AlH_6 = 3LiH + Al + 3/2H_2 \quad \text{(R2)}$$

$$3LiH + 3Al = 3LiAl + 3/2H_2 \quad \text{(R3)}$$

The last reaction (R3) occurs at high temperature (400 °C) and is not considered practical for hydrogen storage applications.

The decomposition temperatures for the first and second reactions are reported to be between 150 and 175 °C and between 180 and 220 °C, respectively.[15] Both reactions are heat-rate dependent and can be reduced to 112 °C for reaction R1 and 127 °C for reaction R2 using very slow heating rates.[13] By adding 5% $TiCl_3 \cdot 1/3(AlCl_3)$ and VCl_3 additives to $LiAlD_4$, the thermal decomposition temperatures are reduced by 60 and 50 °C, respectively.[17] So far, full reversibility of the lithium alanate system has not been demonstrated.

Several experimental techniques, ranging from X-ray diffraction (XRD)[18−22] to nuclear magnetic resonance (NMR),[10,21] have been used to elucidate the role of the additives in the reactions. Nevertheless, there is still no clear understanding of whether the Ti is segregated at the surface of the alanates, the

* Corresponding author. Fax: +47 73 59 77 10. E-mail: randi.holmestad@phys.ntnu.no.
[†] Norwegian University of Science and Technology.
[‡] SINTEF Materials and Chemistry.
[§] Institute for Energy Technology.
[||] McMaster University.

10.1021/jp045083a CCC: $30.25
Published on Web 02/17/2005

TABLE 1: Samples Studied in Different Steps of the Decomposition Process

no.	sample	condition
1	$LiAlD_4 + 2\%TiCl_3 \cdot 1/3(AlCl_3)$	ball milled (BM)
2	$Li_3AlD_6 + 2Al + 2\%TiCl_3 \cdot 1/3(AlCl_3)$	thermal decomposition of 1 (after reaction R1)
3	$LiD + Al + 2\%TiCl_3 \cdot 1/3(AlCl_3)$	thermal decomposition of 1 (after reaction R2)
4	$LiAlD_4 + 2\%VCl_3$	BM
5	$Li_3AlD_6 + 2Al + 2\%VCl_3$	thermal decomposition of 4 (after reaction R1)
6	$LiD + Al + 2\%VCl_3$	thermal decomposition of 4 (after reaction R2)
7	$Li_3AlD_6 + 2Al + 2\%TiCl_3 \cdot 1/3(AlCl_3)$	thermal decomposed $LiAlD_4$ (after reaction R1), then BM with the additive
8	$LiD + Al + 2\%TiCl_3 \cdot 1/3(AlCl_3)$	thermal decomposed $LiAlD_4$ (after reaction R2), then BM with the additive

Ti substitutes with the Na/Li or Al atoms, or other phases are formed. Analytical electron microscopy can provide key information about the spatial distribution of these elements, but several problems have limited the number of such studies. Due to the high sensitivity of the alanates to the electron beam and their instability in air, special sample handling precautions need to be followed prior to the microscopy studies and fast automated acquisition methods must be used in order to provide reliable data. However, some work has been done using transmission electron microscopy (TEM) and scanning electron microscopy (SEM) to study $LiAlH_4$ during different steps of the decomposition process.[23]

The purpose of this research is to study the microstructure of $LiAlD_4$ with $TiCl_3 \cdot 1/3(AlCl_3)$ and VCl_3 added during different stages of the decomposition process using a range of analytical electron microscopy techniques. The distribution of Al and additives within the particles were analyzed using electron energy loss spectroscopy (EELS) imaging methods in the scanning transmission electron microscopy (STEM) mode with simultaneously acquisition of the energy-dispersive X-ray spectra (EDS). Energy filtered transmission electron microscopy (EFTEM) was also used to map the spatial distribution of the elements in the sample. Results from $LiAlD_4$ decomposed and then ball milled with additives are compared to $LiAlD_4$ samples mixed with the additives by ball milling prior to decomposition. Finally, a comparison between the effects of Ti and V additives on the structure is made.

Experimental Methods

$LiAlD_4$ (>98% purity), $TiCl_3 \cdot 1/3(AlCl_3)$ (99.99%), and VCl_3 (99.99%) were obtained as powders from Sigma-Aldrich Chemicals and stored under Ar atmosphere. Commercial $LiAlD_4$ was used instead of $LiAlH_4$ because it is nearly a single-phase material (0.2 wt % LiCl) and was available from earlier neutron diffraction studies. All handling of the samples was done in dry N_2/Ar atmosphere in a glovebox (<5 ppm O_2) to minimize reaction with moisture and oxygen.

Typically 0.5−1 g of the material was mechanically processed by ball milling for 5 min at a gyration rate of 400 rpm using a Pulverisette 7 ball mill. A hardened steel vial of 12 cm^3 sealed under argon with three steel balls (3 g each) was used. The ball milling vial had a rubber seal between the vial and the lid, and they were held together with a clamp. The vial was assembled and disassembled in the glovebox, and the ball milling was performed at room temperature and atmospheric pressure.

Samples of 2 mol % $TiCl_3 \cdot 1/3(AlCl_3)$ and VCl_3 were introduced to the alanate phase by ball milling at different stages in the decomposition process. Table 1 gives an overview of the eight samples studied in this work. Only results from samples 1, 3, 4, and 8 are presented in this paper. Details concerning thermal decomposition spectroscopy and X-ray diffraction of $LiAlD_4$ with Ti and V additives are presented elsewhere.[17]

Electron microscopy samples were prepared in a glovebox by mechanical grinding of the powder in a silicate crucible and spreading the fine powder on a holey carbon film supported on a copper grid. The grid was placed directly on the TEM sample holder in the glovebox and finally transferred to the TEM by means of a vacuum transfer container. To prevent exposure to air during insertion of the sample into the microscope, a removable glovebag device was placed around the specimen exchange system of the TEM column and maintained with N_2/Ar overpressure. The bag was flushed with N_2/Ar for at least 5 min before use. The oxygen level in the glovebag was not quantified. Samples were then removed from the vacuum transfer container in the glovebag and inserted in the TEM column without exposure to air. Electron microscopy studies were performed with a JEOL2010F TEM equipped with a field emission gun (FEG) operated at 200 kV. The system is equipped with a Gatan imaging filtering (GIF) system (Tridiem model) for the acquisition of electron energy loss spectra. Measurements were performed in STEM mode at a camera length of 40 cm with a subnanometer electron probe size. Energy resolution, defined as the full width at half-maximum of the zero loss peak, was around 1.2 eV. EELS measurements were performed with an energy dispersion of 0.2 eV/channel, which allows the simultaneous acquisition of the Ti $L_{2,3}$ edges and the O K edge. The recording times for the acquisition of spectra were selected between 2 and 8 s for the low-energy core-loss region (Ti $L_{2,3}$, O K edges) and about 20 s for the high-energy core-loss region (Al K). The Li K edge is at 55 eV, and it was very difficult to detect due to the presence of plasmon peaks. The background for each spectrum was subtracted by using a power law function.[24]

To provide the spatial distribution of elements and their chemical states, we used the spectrum imaging (SI) technique,[25,26] where an energy loss spectrum and an energy-dispersive X-ray spectrum are acquired at each pixel of a rastered area. With the detailed energy loss distribution available at each pixel, we can provide information on both the spatial distributions of the elements and the chemical state, by analyzing the fine structure modulations at the edge threshold of the EELS spectra. The EDS data give additional information about chemical composition. Using well-defined integration windows, it is possible to map the distribution of the elements with a particular chemical state. Characteristic maps for Ti and TiO_2 were generated by integrating their edges in a 15 and 8 eV wide window at the Ti and O K edge, respectively (the O K edge for TiO_2 has an unique prepeak feature at about 532 eV which allows us to identify this phase). Characteristic maps for Al_2O_3 were extracted using a 10 eV signal integration window at the O K edge where there is no overlap with the features corresponding to the TiO_2 phase. Almost the same windows were used to generate the maps for V and V oxide. The use of the spectrum imaging technique allowed the rapid acquisition of several spectra over a scanned area with minimal overhead time between the adjacent data points.

The size of the images (the numbers of pixels) was kept relatively small to minimize the effect of sample drift, which

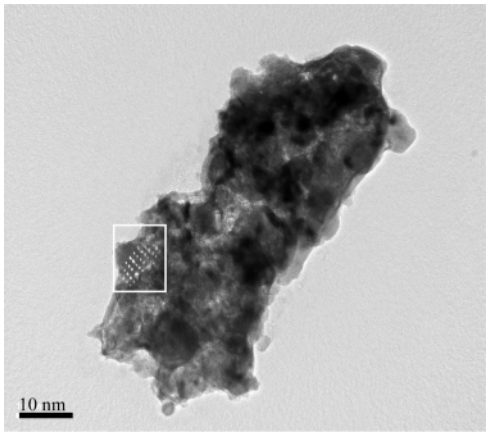

Figure 1. Bright field image of Li_3AlD_6 + 2Al containing $TiCl_3$·1/3($AlCl_3$) additive after EELS spectrum image acquisition, showing effect of beam damage in the selected area.

was corrected automatically during acquisition. The pixel step was selected so as to reduce the overlap between the irradiated areas at each pixel. The exposure time for the EDS signal was typically 3 s/pixel. The electron loss near-edge structure (ELNES) feature energies were calibrated relative to the C edge. We defined the onset for all the EELS features as the inflection point in the intensity rise at the edge.

We used the energy filtered TEM spectrum image technique where a series of energy filtered images is acquired over a large energy range. This provides complementary information with respect to the scanning spectrum imaging method. Each image is formed from a defined energy window. This approach gives a better spatial sampling at the expense of an increased dose to the irradiated area. All the acquisition and data analysis were carried out in the standard Digital Micrograph environment with spectrum imaging scripts (SI and EFTEM spectrum imaging) provided by Gatan.

Due to the irregular shape of the particles, all the EELS spectra were obtained near the edges ($t/\lambda < 0.5$). Electron beam damage was observed in some of the particles as holes left after the acquisition of maps, as shown in the rastered area in Figure 1. Such effects did not appear to affect the information on the chemical composition for metallic elements, although the formation of molecular oxygen has occasionally been detected. It was not possible to quantify the degree of this damage; however, most of the particles appeared reasonably stable under the electron beam. It is possible that the decomposition was caused by localized beam heating, which will vary from position to position and from particle to particle.

Results and Discussion

Figure 2 shows a dark field (DF) STEM image of $LiAlD_4$ with $TiCl_3$·1/3($AlCl_3$) directly after ball milling (sample 1). An EELS spectrum taken in the position indicated by "x" shows the Cl $L_{2,3}$, C K, Ti $L_{2,3}$, and O K edges. The presence of Ti and Cl together suggests that the $TiCl_3$·1/3($AlCl_3$) additive has not completely decomposed. EELS spectra taken from other positions in the particle indicated the presence of TiO_2. The presence of the separate TiF_3 phase was observed also in $NaAlH_4$ samples after the initial ball milling process with this additive.[27]

A DF STEM image of a LiD + Al sample, decomposed first upon heating (reaction R2) and then mixed by ball milling with 2 mol % $TiCl_3$·1/3($AlCl_3$) additive (sample 8), is shown in Figure 3.

EELS spectra extracted from the positions indicated "a" and "b" in Figure 3 are displayed in Figure 4. Figure 4a shows the Ti $L_{2,3}$ edge, with its two intense white lines, and the O K edge. The first peak on the O K edge is attributed to the TiO_2 phase and can be related to the existence of hybridized O 2p−Ti 3d vacant orbitals.[28] The characteristic maps for Ti and TiO_2 are shown in Figure 5a,b. Figure 4b shows the fine structure corresponding to Al_2O_3, but at this energy resolution we were not able to distinguish between variants of the Al_2O_3 phase or whether Li is also present.

The Ti $L_{2,3}$ edges at 456 eV are barely visible in this spectrum. The characteristic map for Al_2O_3 is presented in Figure 5d. There is a good correlation between the Ti maps obtained from EELS (Figure 5a) and EDS (Figure 5c), suggesting the area is sufficiently thin and the changes in the intensity are not due to thickness variations.

Closer examination of the characteristic maps suggests that Ti is concentrated more at the edges of the particle. The strong correlation between the EELS TiO_2 map and the Ti L map suggests that most of the Ti is oxidized. The Al signal extracted from the EDS data (Figure 5e) has a completely different distribution than the Ti signal in the scanned area. In addition, no evidence of bonding between Al and Ti atoms is found from inspection of the ELNES of the Ti $L_{2,3}$ edges at this energy resolution. EELS is most reliable for analysis of thin areas and cannot be used unambiguously to ascertain the location of the Ti where the sample is thicker. However, the complementary

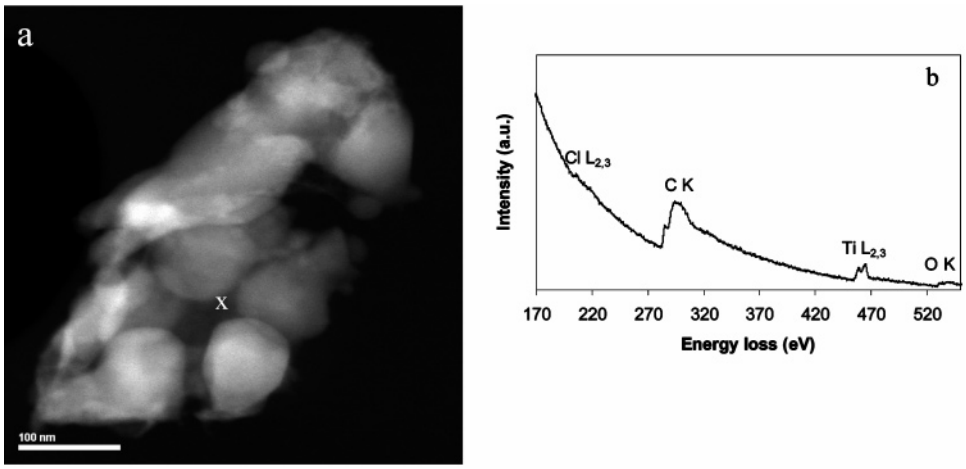

Figure 2. (a) Dark field STEM image of $LiAlD_4$ ball milled with $TiCl_3$·1/3($AlCl_3$) additive and (b) EELS spectrum from the position indicated by "x".

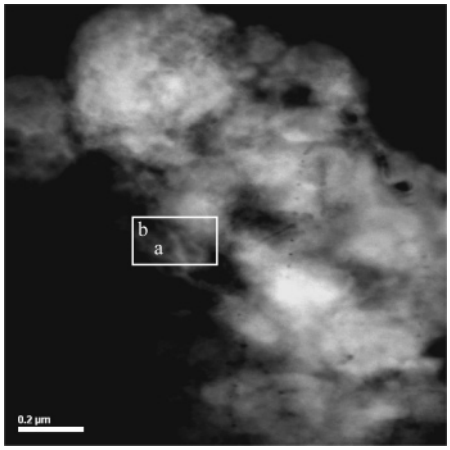

Figure 3. Dark field STEM image of LiD + Al (decomposed first) with 2 mol % $TiCl_3$·1/3($AlCl_3$) additive. An indicated 256 × 135 nm area was used to acquire EELS and EDS signals shown in Figure 5. EELS spectra from the "a" and "b" positions are plotted in Figure 4.

information from EDS also supports the conclusion that the Ti is concentrated at the edges. The Al_2O_3 signal seems to be more pronounced in the thinnest part of the particle, close to the edges (see the top left corner of the rastered area in Figure 5d), although some overlap with the TiO_2 signal is possible where strong contributions from the TiO_2 signal are present. Despite the precautions taken to prevent the exposure of the material to oxygen during sample handling, Ti oxide and alumina phases are present in all particles of this sample.

The DF STEM image of the LiD + Al sample, resulting from the thermal decomposition of $LiAlD_4$ ball milled with $TiCl_3$·1/3($AlCl_3$) (sample 3), is presented in Figure 6a. An EDS spectrum (Figure 6b) taken in the position indicated by the "x" shows the presence of Al, Ti, O, and Cl. The related EELS spectrum obtained from the same position (not shown here) presents features similar to those of the one in Figure 4a and therefore indicates the presence of TiO_2.

After 4 months storage in the glovebox, there was evidence that the sample had degraded. In two particles, which are indicated in the right corner of Figure 7, only a small amount of alumina was detected, at the edges of the particles. EELS spectra from these particles are plotted in Figure 7 and illustrate the chemical state information that can be obtained using EELS. Examination of the near-edge structure and comparison with published data[29,30] suggest that there are two different phases of titanium oxide. The energy position of two relatively sharp peaks for the O K edge show similar features for both rutile and anatase TiO_2. There are, however, differences in the near-edge structure of these two compounds at about 540 eV where the rutile spectrum has three peaks and the anatase has only two (as indicated by dashed lines).

A sample of $LiAlD_4$ ball milled with 2% VCl_3 was studied (sample 4). A dark field STEM image of sample 4 is presented in Figure 8. The highlighted area is used to acquire EELS and EDS signals and to obtain the characteristic maps. EELS spectra from two neighboring positions in the selected area are shown in Figure 9.

The spectrum taken in position "1" shows the Al_2O_3 peak at the O K edge, and the spectrum in position "2" shows the V $L_{2,3}$ edges. On the basis of the fine structure, we can say that the vanadium is oxidized, but it is not possible to distinguish whether VO or V_2O_3 is present, given the similarity of the O K edge for these two compounds.[30] In position "2", a spectrum was also taken in the high-loss region (Al K edge at 1560 eV), which indicates that metallic Al is present.

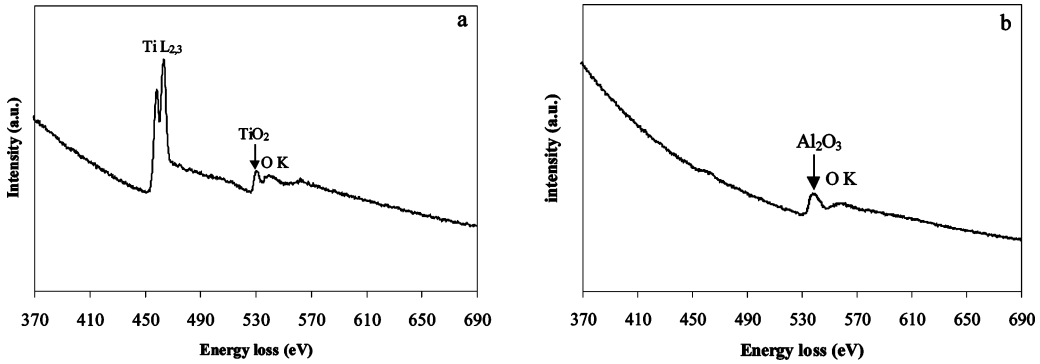

Figure 4. EELS spectra from areas "a" and "b" in Figure 3 (a) Ti $L_{2,3}$ edges and O K edge typical for TiO_2. (b) O K edge for Al_2O_3.

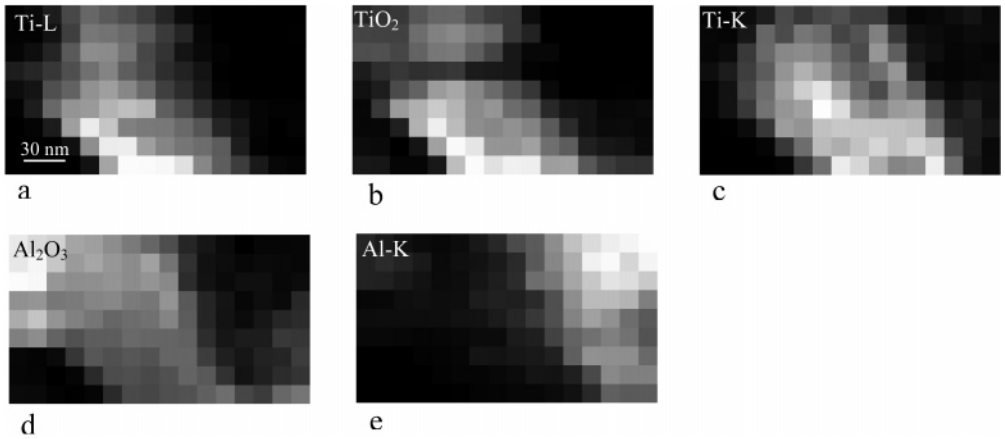

Figure 5. Characteristic maps generated for (a) $TiL_{2,3}$ edges from EELS, (b) TiO_2 from EELS, (c) Ti K peak from EDS, (d) Al_2O_3 from EELS, and (e) Al K peak from EDS.

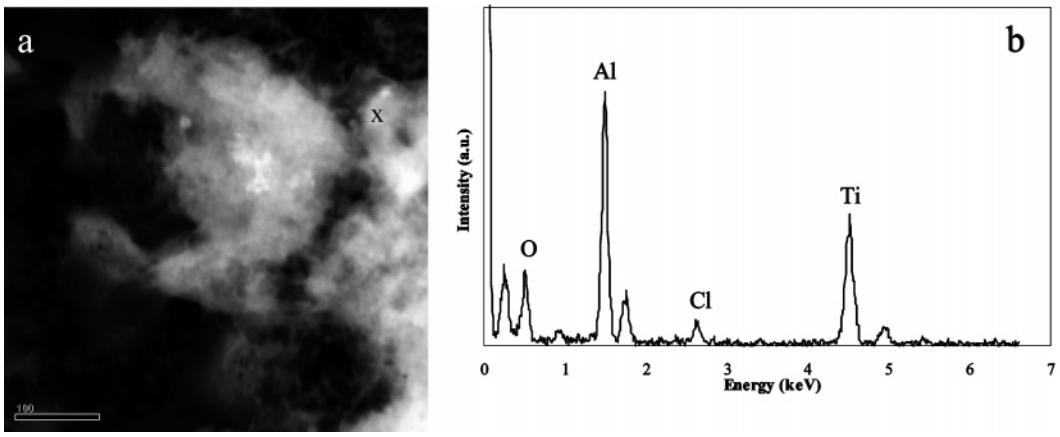

Figure 6. (a) Dark field STEM image of LiD + Al with $TiCl_3 \cdot 1/3(AlCl_3)$ additive and (b) EDS spectrum from the position indicated by "x".

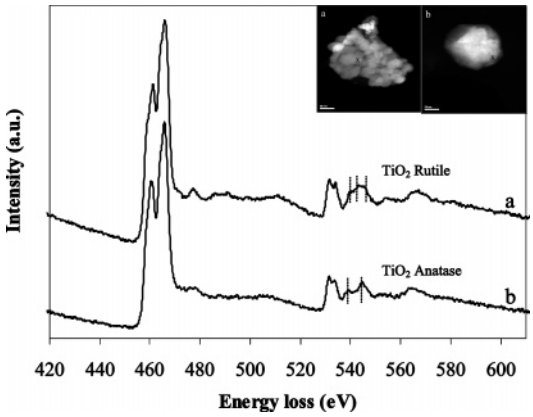

Figure 7. EELS spectra taken from the position indicated by "x" in the two particles in the top right corner, showing two types of TiO_2. The dashed lines indicate the position of the peaks, which give the difference between the types of oxide.

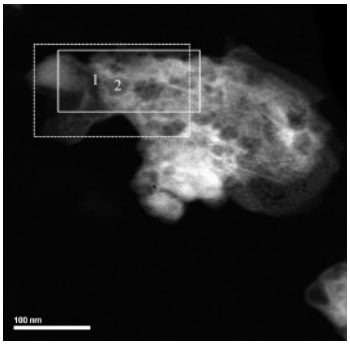

Figure 8. Dark field STEM image of $LiAlD_4$ with VCl_3 additive. The spectra in Figure 9 are from the positions indicated in the smaller marked area. The larger dashed area was used to acquire EFTEM maps (Figure 10). The solid line rectangle was used to acquire the characteristic maps (Figure 11).

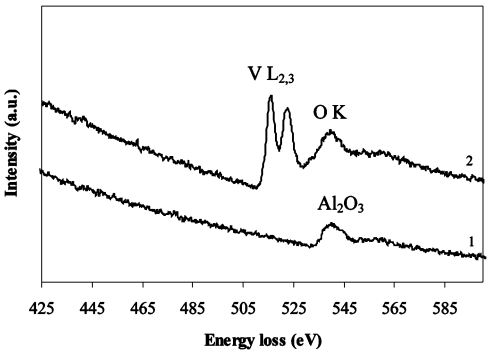

Figure 9. EELS spectra taken in positions "1" and "2" in Figure 8 showing V $L_{2,3}$ and O K edges.

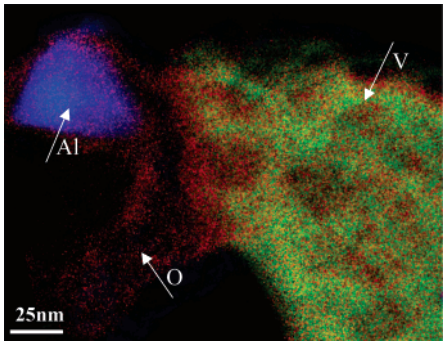

Figure 10. Color-coded image resulting from superposition of the three maps for O (red), V (green), and Al (blue). Strong overlap of the O and V signals gives rise to the yellow region. The area selected here corresponds to the dashed area in Figure 8.

Energy filtered images were taken to provide a better sampling of the elemental distribution of Al, O, and V in the larger dashed area in Figure 8. Images of Al, V, and O were obtained over two loss regimes, one for the Al L edge and another for V and O edges using a 5 eV slit. A color-coded elemental map showing the O (red), V (green), and Al (blue) is presented in Figure 10 as an RGB image. The Al is highly concentrated in the left corner of the image. The oxygen signal is present at a low level everywhere in the particle, and it is strongly correlated to the V and Al signals. We also expect that the oxygen signal is correlated with the Li distribution, which is not detected in our work. The fact that the oxygen and vanadium signals coincide gives rise to the yellow areas resulting from the overlap of the red and green colors in the map. This result is confirmed by the EELS point spectra selected from spectrum images, which indicate the presence of vanadium oxide and Al_2O_3 in the particle.

The characteristic maps for vanadium and vanadium oxide are shown in parts a and b of Figure 11. The strong correlation between V and V oxide in the selected area suggests that most of the V is oxidized. On the basis of the near-edge structure corresponding to the Al_2O_3, as presented in Figure 9, we generated an Al_2O_3 map (Figure 11c). A complementary Al map was also generated using the Al K peak detected from the EDS signal (Figure 11d). On the basis of EELS and EDS maps, it is clear that the location of V is anticorrelated with the position of Al in the scanned area. In this respect, there are strong similarities in the behavior of the additive in the samples containing Ti and V. The location of the strong Al signal in the

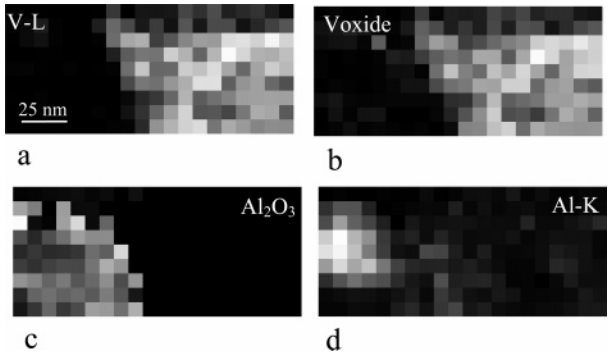

Figure 11. Characteristic maps generated by (a) V $L_{2,3}$ edges in EELS, (b) V oxide in EELS, (c) Al_2O_3 in EELS, and (d) Al K edge from EDS.

EDS map corresponds to the particle (blue color in Figure 10) detected in the EFTEM spectrum image. The V and V oxide positions in the EELS spectrum image also correlate with the ones detected in the RGB image obtained by EFTEM maps. The same experiments were performed on lithium alanates containing 2 mol % VCl_3 additive. All the samples with this additive studied during the decomposition process showed an uneven distribution of the transition metal element in the particles. Cl and Al are also present at different levels in almost all the particles, while vanadium is found in very high concentration in just a few of them. This suggests that the V is not uniformly distributed during processing.

All the samples listed in Table 1, in different stages of the decomposition process and containing two different types of additives, have been analyzed following the procedures illustrated for samples 1, 3, 4, and 8. Even though all the EELS data were acquired in small regions near the edges of the particles, they were consistent for all the samples studied in different stages of the decomposition process. No significant changes regarding the distribution of the elements between the starting material and after reactions R1 and R2 were noticed for either Ti- or V-containing samples. An interesting difference, however, was observed in the case of the distribution of the Ti added by ball milling before and after the decomposition process (samples 3 and 8). Ti seems to be much more uniformly distributed in the latter case, i.e., if the sample is heated before the transition metal element is added. The reason for this is unclear. If Ti is initially distributed at the surface of the alanate particles, ball milling prior to addition can cause more concentration of the additives. Alternatively, there may be a chemical effect leading to different behaviors for $LiAlD_4$ and $LiD + Al$. By comparison, V was found to be highly concentrated in just a few of the particles examined in the samples containing this additive (samples 4−6). Thermal decomposition spectroscopy for these samples suggested two different additive behaviors leading to the reduction of the decomposition temperature.[17] From this point of view, VCl_3 appears to be a better candidate than $TiCl_3 \cdot 1/3(AlCl_3)$. From our results, it is difficult to say whether the opportunities to enhance the decomposition kinetics are better for V than for Ti because V is highly concentrated in the particles. The mechanism behind the kinetics enhancements is still very poorly understood, and the additives do not appear to behave in the same way.

The role of the oxides has not been discussed much in the literature. Moreover, the X-ray studies do not report the presence of any oxides in this type of material. It is possible that some of this oxygen was introduced during the ball milling process since the only sample with low oxygen content was pure $LiAlD_4$, which was not ball milled before examination. Another possibility is that the sample is more reactive after ball milling, due to a lager surface/volume ratio of the particles. The different types of oxides reported in this study may influence the kinetics of the process, particularly where the oxide forms preferentially at the sample surface and where the additive has a different oxidation state.

Conclusions

The microstructure of the alanate $LiAlD_4$, with 2 mol % $TiCl_3 \cdot 1/3(AlCl_3)$ and 2 mol % VCl_3 additives, was studied during different stages of decomposition using EELS, EDS, and EFTEM. This demonstrates that these techniques can be used to study the chemistry of these materials down to the nano scale. The results showed that the distribution of the Al in all the particles anticorrelates with the positions of the additives after ball milling. Al_2O_3 was present in all the investigated particles, in the majority of them forming a thin layer at the surface. Rutile and anatase TiO_2 were found in the samples containing Ti additive. It has been shown that EELS can probe the chemistry of the material. For all the Ti additive conditions studied, it was found that Ti was distributed relatively uniformly between the particles. However, in the samples containing V, most of the additive was in the form of VO or V_2O_3 and V was found highly concentrated in just a few particles. EELS and EDS mapping suggest that Ti is distributed preferentially at particle surfaces. In high V containing particles the transition metal was present in a significant proportion of the particle bulk. We cannot exclude the presence of lithium oxide.

Acknowledgment. The Norwegian Research Council is gratefully acknowledged for financial support on the project "Hydrogen storage in metal hydrides", Contract No. 135502/431.

References and Notes

(1) Bogdanovic, B.; Schwickardi, M. *J. Alloys Compd.* **1997**, *253*, 1.
(2) Jensen, C. M.; Zidan, R.; Mariels, N.; Hee, A.; Hagen, C. *Int. J. Hydrogen E* **1999**, *24*, 461.
(3) Zidan, R. A.; Takara, S.; Hee, A. G.; Jensen, C. M. *J. Alloys Compd.* **1999**, *285*, 119.
(4) Zaluska, A.; Zaluski, L.; Strom-Olsen, J. O. *J. Alloys Compd.* **2000**, *298*, 125.
(5) Finholt, A. E.; Bond, A. C., Jr.; Schlesinger, H. I. *J. Am. Chem. Soc.* **1947**, *69*, 1199.
(6) Garner, W. E.; Haycock, E. W. *Proc. R. Soc. London, Ser. A* **1952**, *A211*, 335.
(7) Block, J.; Gray, A. P. *Inorg. Chem.* **1965**, *4*, 304.
(8) Mal'tseva, N. N.; Golovanova, A. I. *Russ. J. Appl. Chem.* **2000**, *73*, 747.
(9) Chen, J.; Kuriyama, N.; Xu, Q.; Takeshita, H. T.; Sakai, T. *J. Phys Chem. B* **2001**, *105*, 11214.
(10) Balema, V. P.; Wiench, J. W.; Dennis, K. W.; Pruski, M.; Pecharsky, V. K. *J. Alloys Compd.* **2001**, *329*, 108.
(11) Løvvik, O. M.; Opalka, S. M.; Brinks, H. W.; Hauback, B. C. *Phys. Rev. B* **2004**, *69*, 134117.
(12) Hauback, B. C.; Brinks, H. W.; Fjellvåg, H. *J. Alloys Compd.* **2002**, *346*, 184.
(13) Brinks, H. W.; Hauback, B. C.; Norby, P.; Fjellvåg, H. *J. Alloys Compd.* **2003**, *351*, 222.
(14) Mikheeva, V.; Arkhipov, S. *Zh. Neorg. Khim.* **1967**, 12 2025.
(15) Dymova, T. N.; Konoplev, V. N.; Aleksandrov, D. P.; Sizareva, A. S.; Silina, T. A. *Koord. Khim.* **1995**, *21*, 175.
(16) Dilts, J.; Ashby, E. *Inorg. Chem.* **1972**, *11*, 1230.
(17) Blanchard, D.; Brinks, H. W.; Hauback, B. C.; Norby, P. *Mater. Sci. Eng. B* **2004**, *108*, 54.
(18) Brinks, H. W.; Jensen, C. M.; Srinivasan, S. S.; Hauback, B. C.; Blanchard, D.; Murphy, K. *J. Alloys Compd.* **2004**, *376*, 215.
(19) Majzoub, E. H.; Gross, K. J. *J. Alloys Compd.* **2003**, *356*, 363.
(20) Gross, K.; Sandrock, G.; Thomas, G. *J. Alloys Compd.* **2002**, *330*, 691.

(21) Bogdanovic, B.; Felderhoff, M.; Germann, M.; Hartel, M.; Pommerin, A.; Schuth, F.; Weidenthaler, C.; Zibrowius, B. *J. Alloys Compd.* **2003**, *350*, 246.

(22) Fichtner, M.; Fuhr, O.; Kircher, O.; Rothe, J. *Nanotechnology* **2003**, *14*, 778.

(23) Andrei, C. M.; Walmsley, J. C.; Brinks, H. W.; Holmestad, R.; Blanchard, D.; Hauback, B. C. *J. Alloys. Compd.*, in press.

(24) Egerton, R. F. *Electron Energy Loss Spectroscopy in the Electron Microscope*, 2nd ed.; Plenum: New York, 1996.

(25) Jeanguillaume, C.; Colliex, C. *Ultramicroscopy* **1989**, *28*, 252.

(26) Bouchet, D.; Colliex, C.; Flora, P.; Krivanek, O.; Mory, C.; Tence, M. *Microsc. Microanal. Microstruct.* **1990**, *1*, 443.

(27) Andrei, C. M.; Walmsley, J. C.; Brinks, H. W.; Holmestad, R.; Jensen, C. M.; Hauback, B. C. *Appl. Phys. A* **2005**, *80*, 709.

(28) Kurata, H.; Lefevre, E.; Colliex, C.; Brydson, R. *Phys. Rev. B* **1993**, *47*, 13763.

(29) Brydson, R.; Sauer, S.; Engel, W.; Thomas, J. M.; Zeitler, E.; Kosugi, N.; Kuroda, H. *J. Phys. Condens. Matter* **1989**, *1*, 797.

(30) Chen, J. G. *Surf. Sci. Rep.* **1997**, *30*, 1.